Progress In Electromagnetics Research M, Vol. 30, 225–238, 2013

AN ANALYTIC EXPRESSION FOR NEAR-FIELD ANGULAR GLINT PREDICTION OF RADAR SENSOR USING FAR-FIELD SCATTERING CENTERS MODELS

Jianpeng Fan, Shijie Fan, Hongqi Fan*, and Huaitie Xiao

National Key Laboratory of Automatic Target Recognition (ATR), National University of Defense Technology, Changsha, Hunan, P. R. China

Abstract—As an important signature of the radar target, the angular glint effects on radar sensor mainly arise at close distance, especially at target near field. However, the current prediction methods of angular glint are mostly based on the far field condition. This paper presents a prediction technique of near field angular glint based on the scattering center model to solve this problem. Firstly, the near field backscattering is represented based on far-field scattering center model. Then by solving the derivative of the backscattering phase vs. the position vector of the observer, including incident angles and range, we get the exact expression of angular glint at near field. Next, the exact expression is approximated and simplified in the range of terminal guidance. Finally, the factors affecting near-field angular glint are analyzed using numeric simulation, and the error comparison between the exact and approximate expression is also provided. It is concluded that the expression in [1] is the approximation of ours at far field under certain polarization, and the simplified expression has a well precision in the range of terminal guidance. All these results provide the theoretical basis for the prediction of near field angular glint and its signature research.

1. INTRODUCTION

As is well known, angular glint is a radar target signature in equal importance compared with radar cross section (RCS), and its effects on radar sensor mainly arise at target near field. As the radar homing guidance technique rapidly develops, target angular glint signature

Received 21 March 2013, Accepted 29 April 2013, Scheduled 7 May 2013

* Corresponding author: Hongqi Fan (fanhongqi@tsinghua.org.cn).

attracts an increasing attention [1, 2]. When missile approaches target, on the one hand angular glint becomes the main tracking error source of the guidance system [3, 4]; on the other hand, as a kind of target signature, angular glint can provide abundant information on target motion model identification, target recognition, etc. [5]. Therefore, setting up the prediction model of angular glint has great realistic significance on the angular glint investigation, mitigation, exploitation and so on.

At present, two theories namely wavefront distortion and energy flux density tilt are usually adopted to explain the generation of angular glint, corresponding to two calculation methods-phase gradient method and Poynting vector method. Reference [1] proves that the two methods are equivalent under the geometrical optics approximation condition, and derives the calculating formula based on the far field condition. However, in the range of terminal guidance, the approximate condition for most terminal guidance radars that work in the optical region cannot be satisfied. For instance, when a radar with $\lambda = 5\,\mathrm{cm}$ in wavelength acts on a target with $d = 20\,\mathrm{m}$ in maximum size, the far field condition ($r > 2d^2/\lambda$) requires a distance larger than 16 km. If the far field condition cannot be satisfied, is the calculating formula in [1] applicable? Furthermore, how to calculate the near-field angular glint?

To answer these questions, in this paper firstly we derive the backscattering expression of target under the near field condition based on the scattering center model in the optical region. Then, by solving the derivative of the backscattering phase vs. the position vector of the observer, we obtain the exact expression of angular glint at near field based on phase gradient method, and show that the expression in [1] is the far-field approximation of ours under certain polarization. Considering the exact expression is fairly complicated, we simplify it combined with the typical range of terminal guidance radar sensor. Finally, simulations are implemented to validate our expression.

2. PROBLEM DESCRIPTION

As both the theoretical calculation and experimental measurement demonstrate, in the optical region, the total electromagnetic scattering of target can be considered as being made up by the electromagnetic scattering from some local positions, which usually are called scattering centers [1]. Scattering center is an important feature of the electromagnetic scattering in the optical region and represents the scattering characteristics of the surrounding local regions. Thus, in this study, we assume that in the range of the considered distance,

whether target locates in the far-field of radar or not, each scattering center is in the local region that satisfies the far-field condition. In effect, the assumption is widely adopted by the study of the near-field target characteristics [6, 7]. Under the assumption, the far-field scattering center model can be employed to investigate the target characteristics at near field. Bhalla and Ling [8] used the far-field scattering center model based on the SBR method to estimate the near-field RCS, and obtained results that are fairly consistent with electromagnetic computing and measured data, which is a further evidence of the assumption rationality. Actually, assume 20 scattering centers distribute uniformly on a target with 20 m in size, and then each scattering center can represent a region with about 1 m in size. That distance under the far-field condition for the radar with $\lambda = 5$ cm in wavelength is 40 m, far less than the radar blind range.

Based on the above assumption, when the far-field condition is not satisfied, on the one hand, the incident electromagnetic waves cannot be treated as plane waves, but spherical waves, as generally the radar aperture D is far less than the target size; on the other hand, the local region in which each scattering center lies satisfies the far-field approximation, and thus both the incident and scattering waves can be treated as plane waves.

As Figure 1 displays, in the target coordinate system, the position and orientation of the radar antenna can be uniquely determined by $[r, \varphi, \theta, \varepsilon_x, \varepsilon_z, \varepsilon_y]^{\mathrm{T}}$, where $[r, \varphi, \theta]^{\mathrm{T}}$ is the antenna position vector $\mathbf{r}$ in the spherical coordinates form, $\{\varepsilon_x, \varepsilon_y, -\varepsilon_z\}$ represents the three rotating angles from the antenna coordinates $(x, y, z)_{\mathrm{R}}$ to the incident coordinates $(\hat{k}_c^i, \hat{\mathbf{E}}_{c\parallel}^i, \hat{\mathbf{E}}_{c\perp}^i)$ in the order XZY; as with the terminal guidance system, ε_x is the polarization rotating angle related to the reference polarized direction, ε_y and ε_z are the boresight error along the y and z direction respectively, and $[r_n, \varphi_n, \theta_n]^{\mathrm{T}}$ is the spherical

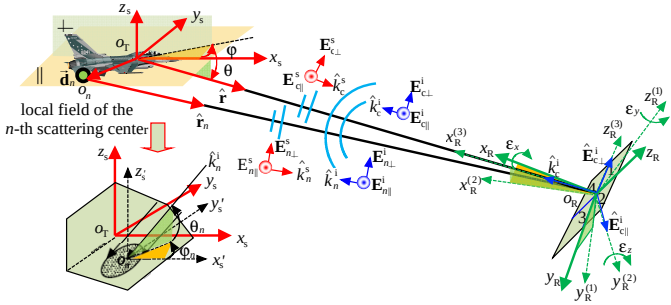

Figure 1. Sketch map of the incident-scattering relationship based on the near-field condition.

coordinates representation in the target coordinate system of the distance vector $\mathbf{r}_n$ between the nth scattering center and the radar.

Let P_t, G, $F(\cdot)$, $\mathbf{h}^r$ and $\mathbf{h}^i$ be the radar transmit power, antenna gain, antenna pattern function, and the transmitting and receiving polarization respectively, ψ_c, ψ_n denote the angles between $\overrightarrow{o_{\mathrm{R}}o_{\mathrm{T}}}$, $\overrightarrow{o_{\mathrm{R}}o_n}$ and the electrical boresight of antenna respectively, $\mathbf{R}(\varepsilon_x)$ denote the polarization rotation matrix, and $\mathbf{S}_{n,\varphi_n,\theta_n}$ denote the single station line polarization scattering matrix of the nth scattering center in the incident direction (φ_n, θ_n).

Ignoring the time-harmonic factor $e^{j\omega t}$, the scattering intensity at the radar can be formulated as:

$$\mathbf{E}^s = \sqrt{P_t G}(\mathbf{h}^r)^{\mathrm{T}}(\mathbf{R}(\varepsilon_x))^{\mathrm{T}}\left[\sum_n \frac{F^2(\psi_n)}{4\pi {r_n}^2}\mathbf{S}_{n,\varphi_n,\theta_n}\cdot\exp\left(-2jkr_n\right)\right]\mathbf{R}(\varepsilon_x)\mathbf{h}^i \tag{1}$$

Based on the definition of the near-field RCS [9], the near-field scattering matrix $\mathbf{S}$ can be defined as:

$$\mathbf{S}(r,\varphi,\theta,\varepsilon_z,\varepsilon_y,F(\cdot),V,k) = \sum_n \frac{F^2(\psi_n)}{F^2(\psi_c)}\cdot\frac{r^2}{{r_n}^2}\cdot\mathbf{S}_{n,\varphi_n,\theta_n}\cdot\exp(-2jkr_n) \tag{2}$$

where $r = |\mathbf{r}|$, $r_n = |\mathbf{r}_n t| = |\mathbf{r} - \mathbf{d}_n|$, $\psi_c = \arccos\left(\cos(\varepsilon_y)\cos(\varepsilon_z)\right)$, $\psi_n = \arccos(-\hat{\mathbf{x}}_{\mathbf{R}}\cdot\hat{\mathbf{r}}_n)$, and V stands for the physical structure of target. Obviously, $\mathbf{S}$ represents the full polarization scattering matrix in the direction (φ, θ). In comparison with the far-field scattering matrix, it not only is related to target physical structure V, wavenumber k, and incident angle (φ, θ), but also depends on the distance r between radar and target center, antenna boresight error ε_z, ε_y and antenna pattern $F(\cdot)$.

Substituting $\mathbf{S}$ into $\mathbf{E}^s$, the scattering intensity can be rewritten as:

$$\mathbf{E}^s = \frac{F^2(\psi_c)\sqrt{P_t G}}{4\pi r^2}(\mathbf{h}^r)^{\mathrm{T}}(\mathbf{R}(\varepsilon_x))^{\mathrm{T}}\mathbf{S}\mathbf{R}(\varepsilon_x)\mathbf{h}^i \tag{3}$$

3. NEAR-FIELD ANGLE GLINT EXPRESSION

For simplicity, we use $\mathbf{R}$ to stand for the polarization rotation matrix $\mathbf{R}(\varepsilon_x)$, and represent $\mathbf{S}$ in a complex form $\mathbf{S} = \mathbf{S}^{\mathrm{Re}} + j\cdot\mathbf{S}^{\mathrm{Im}}$. In the terminal guidance process, the boresight error ψ_c approximately equals to tracking error, generally in the mil order. Thus, we consider the situation with $\psi_c = 0$.

The phase function of $\mathbf{E}^s$ in (3) can be expressed as:

$$\Phi(r,\theta,\varphi) = -\arg(\mathbf{E}^s) = -\arctan\frac{V_N}{U_N} = -\arctan\left(\frac{(\mathbf{R}\mathbf{h}^r)^{\mathrm{T}}\mathbf{S}^{\mathrm{Im}}\mathbf{R}\mathbf{h}^i}{(\mathbf{R}\mathbf{h}^r)^{\mathrm{T}}\mathbf{S}^{\mathrm{Re}}\mathbf{R}\mathbf{h}^i}\right) \tag{4}$$

where

$$\begin{aligned}\mathbf{S}^{\mathrm{Re}}&=\sum_n F^2(\psi_n)\cdot\frac{r^2}{r_n^2}\cdot\left(\mathbf{S}^{\mathrm{Re}}_{n,\varphi_n,\theta_n}\cos(2kr_n)+\mathbf{S}^{\mathrm{Im}}_{n,\varphi_n,\theta_n}\sin(2kr_n)\right)\\&=\sum_n A_n\cdot\left(\mathbf{S}^{\mathrm{Re}}_{n,\varphi_n,\theta_n}\cos\alpha_n+\mathbf{S}^{\mathrm{Im}}_{n,\varphi_n,\theta_n}\sin\alpha_n\right)=\sum_n\mathbf{S}^{\mathrm{Re}}_n\\\mathbf{S}^{\mathrm{Im}}&=\sum_n F^2(\psi_n)\cdot\frac{r^2}{r_n^2}\cdot\left(-\mathbf{S}^{\mathrm{Re}}_{n,\varphi_n,\theta_n}\sin(2kr_n)+\mathbf{S}^{\mathrm{Im}}_{n,\varphi_n,\theta_n}\cos(2kr_n)\right)\\&=\sum_n A_n\left(-\mathbf{S}^{\mathrm{Re}}_{n,\varphi_n,\theta_n}\sin\alpha_n+\mathbf{S}^{\mathrm{Im}}_{n,\varphi_n,\theta_n}\cos\alpha_n\right)=\sum_n\mathbf{S}^{\mathrm{Im}}_n\end{aligned}\tag{5}$$

Based on the basic principle of the phase gradient method [1], we can obtain the target line glint error as:

$$\begin{aligned}e_\theta&=\frac{\partial\Phi/\partial\theta}{\partial\Phi/\partial r}=\frac{(\mathbf{Rh}^r)^{\mathrm{T}}\left[U_N\sum_n\partial\mathbf{S}^{\mathrm{Im}}_n/\partial\theta-V_N\sum_n\partial\mathbf{S}^{\mathrm{Re}}_n/\partial\theta\right]\mathbf{Rh}^i}{(\mathbf{Rh}^r)^{\mathrm{T}}\left[U_N\sum_n\partial\mathbf{S}^{\mathrm{Im}}_n/\partial r-V_N\sum_n\partial\mathbf{S}^{\mathrm{Re}}_n/\partial r\right]\mathbf{Rh}^i}\\e_\varphi&=\frac{\partial\Phi/\partial\varphi}{\cos\theta\cdot\partial\Phi/\partial r}\\&=\frac{(\mathbf{Rh}^r)^{\mathrm{T}}\left(U_N\sum_n\partial\mathbf{S}^{\mathrm{Im}}_n/\partial\varphi-V_N\sum_n\partial\mathbf{S}^{\mathrm{Re}}_n/\partial\varphi\right)\mathbf{Rh}^i}{\cos\theta\cdot(\mathbf{Rh}^r)^{\mathrm{T}}\left(U_N\sum_n\partial\mathbf{S}^{\mathrm{Im}}_n/\partial r-V_N\sum_n\partial\mathbf{S}^{\mathrm{Re}}_n/\partial r\right)\mathbf{Rh}^i}\end{aligned}\tag{6}$$

where

$$\begin{aligned}\begin{bmatrix}\partial\mathbf{S}^{\mathrm{Re}}_n/\partial r\\\partial\mathbf{S}^{\mathrm{Re}}_n/\partial\varphi\\\partial\mathbf{S}^{\mathrm{Re}}_n/\partial\theta\end{bmatrix}&=\begin{bmatrix}\mathbf{S}^{\mathrm{Im}}_n\partial\alpha_n/\partial r+\mathbf{S}^{\mathrm{Re}}_n\cdot\partial\ln A_n/\partial r\\\mathbf{S}^{\mathrm{Im}}_n\partial\alpha_n/\partial\varphi+\mathbf{S}^{\mathrm{Re}}_n\cdot\partial\ln A_n/\partial\varphi\\\mathbf{S}^{\mathrm{Im}}_n\partial\alpha_n/\partial\theta+\mathbf{S}^{\mathrm{Re}}_n\cdot\partial\ln A_n/\partial\theta\end{bmatrix}\\\begin{bmatrix}\partial\mathbf{S}^{\mathrm{Im}}_n/\partial r\\\partial\mathbf{S}^{\mathrm{Im}}_n/\partial\varphi\\\partial\mathbf{S}^{\mathrm{Im}}_n/\partial\theta\end{bmatrix}&=\begin{bmatrix}-\mathbf{S}^{\mathrm{Re}}_n\partial\alpha_n/\partial r+\mathbf{S}^{\mathrm{Im}}_n\cdot\partial\ln A_n/\partial r\\-\mathbf{S}^{\mathrm{Re}}_n\partial\alpha_n/\partial\varphi+\mathbf{S}^{\mathrm{Im}}_n\cdot\partial\ln A_n/\partial\varphi\\-\mathbf{S}^{\mathrm{Re}}_n\partial\alpha_n/\partial\theta+\mathbf{S}^{\mathrm{Im}}_n\cdot\partial\ln A_n/\partial\theta\end{bmatrix}\end{aligned}\tag{7}$$

$$\begin{bmatrix}\partial\alpha_n/\partial r\\\partial\alpha_n/\partial\varphi\\\partial\alpha_n/\partial\theta\end{bmatrix}=2k\begin{bmatrix}\partial r_n/\partial r\\\partial r_n/\partial\varphi\\\partial r_n/\partial\theta\end{bmatrix}=-2k\frac{r}{r_n}\cdot\begin{bmatrix}\mathbf{d}_n\cdot\hat{\mathbf{r}}/r-1\\\mathbf{d}_n\cdot\hat{\varphi}\cdot\cos\theta\\\mathbf{d}_n\cdot\hat{\theta}\end{bmatrix}\tag{8}$$

$$\begin{bmatrix}\partial\ln A_n/\partial r\\\partial\ln A_n/\partial\varphi\\\partial\ln A_n/\partial\theta\end{bmatrix}=\frac{2}{F(\psi_n)}\cdot\frac{\partial F}{\partial(\cos\psi)}\cdot\begin{bmatrix}\partial(\hat{\mathbf{r}}\cdot\hat{\mathbf{r}}_n)/\partial r\\\partial(\hat{\mathbf{r}}\cdot\hat{\mathbf{r}}_n)/\partial\varphi\\\partial(\hat{\mathbf{r}}\cdot\hat{\mathbf{r}}_n)/\partial\theta\end{bmatrix}$$

$$
\begin{aligned}
&+2\cdot\left(\frac{1}{r}\begin{bmatrix}1\\0\\0\end{bmatrix}-\frac{1}{r_n}\begin{bmatrix}\partial r_n/\partial r\\ \partial r_n/\partial\varphi\\ \partial r_n/\partial\theta\end{bmatrix}\right)\\
&=2\left(\frac{1}{r}\begin{bmatrix}1\\0\\0\end{bmatrix}+\frac{1}{r_n}\cdot\frac{r}{r_n}\begin{bmatrix}\mathbf{d}_n\cdot\hat{\mathbf{r}}/r-1\\ \cos\theta\cdot\mathbf{d}_n\cdot\hat{\varphi}\\ \mathbf{d}_n\cdot\hat{\theta}\end{bmatrix}\right.\\
&\quad\left.-\frac{1}{r_n}\cdot\frac{1}{F(\psi_n)}\cdot\frac{\partial F}{\partial(\cos\psi_n)}\cdot\begin{bmatrix}-1\\ \cos\theta\cdot\mathbf{d}_n\cdot\hat{\varphi}\\ \mathbf{d}_n\cdot\hat{\theta}\end{bmatrix}\right)\\
&=2\left(\frac{{r_n}^2+r\cdot\mathbf{d}_n\cdot\hat{\mathbf{r}}}{r\cdot{r_n}^2}\begin{bmatrix}1\\0\\0\end{bmatrix}\right.\\
&\quad\left.+\frac{1}{r_n}\left(\frac{r}{r_n}-\frac{1}{F(\psi_n)}\cdot\frac{\partial F}{\partial(\cos\psi_n)}\right)\cdot\begin{bmatrix}-1\\ \cos\theta\cdot\mathbf{d}_n\cdot\hat{\varphi}\\ \mathbf{d}_n\cdot\hat{\theta}\end{bmatrix}\right)
\end{aligned}
\tag{9}
$$

Under the far-field condition, when $r\to\infty$, target is in the far field of radar, $\psi_n\to 0$, $r_n/r\to 1$, $A_n\to 1$, and $r-r_n\approx\mathbf{d}_n\cdot\hat{\mathbf{r}}\ll r$. Therefore

$$
\begin{bmatrix}\partial\alpha_n/\partial r\\ \partial\alpha_n/\partial\varphi\\ \partial\alpha_n/\partial\theta\end{bmatrix}\approx -2k\begin{bmatrix}-1\\ \cos\theta\cdot\mathbf{d}_n\cdot\hat{\varphi}\\ \mathbf{d}_n\cdot\hat{\theta}\end{bmatrix};\quad\begin{bmatrix}\partial\ln A_n/\partial r\\ \partial\ln A_n/\partial\varphi\\ \partial\ln A_n/\partial\theta\end{bmatrix}\approx 0 \tag{10}
$$

Substitute (10) into (7), and let the polarization rotation angle ε_x equal to 0, then we can obtain

$$
\left(\mathbf{h}^r,\mathbf{h}^i\right)\in\left\{(\mathbf{h}_i,\mathbf{h}_j)|i,j=1,2,\mathbf{h}_1=\begin{bmatrix}1\\0\end{bmatrix},\mathbf{h}_2=\begin{bmatrix}0\\1\end{bmatrix}\right\} \tag{11}
$$

and (6) can be simplified as

$$
\begin{aligned}
e_\theta&=\frac{U_N\sum\limits_n\partial\left[\mathbf{S}_n^{\mathrm{Im}}\right]_{ij}/\partial\theta-V_N\sum\limits_n\left[\mathbf{S}_n^{\mathrm{Re}}\right]_{ij}/\partial\theta}{U_N\sum\limits_n\left[\mathbf{S}_n^{\mathrm{Im}}\right]_{ij}/\partial r-V_N\sum\limits_n\left[\mathbf{S}_n^{\mathrm{Re}}\right]_{ij}/\partial r}\\
&=-\frac{U_N\sum\limits_n\left[\mathbf{S}_n^{\mathrm{Re}}\right]_{ij}\cdot\mathbf{d}_n\cdot\hat{\theta}+V_N\sum\limits_n\left[\mathbf{S}_n^{\mathrm{Im}}\right]_{ij}\cdot\mathbf{d}_n\cdot\hat{\theta}}{{U_N}^2+{V_N}^2}\\
e_\varphi&=\frac{1}{\cos\theta}\cdot\frac{U_N\sum\limits_n\partial\left[\mathbf{S}_n^{\mathrm{Im}}\right]_{ij}/\partial\varphi-V_N\sum\limits_n\left[\mathbf{S}_n^{\mathrm{Re}}\right]_{ij}/\partial\varphi}{U_N\sum\limits_n\left[\mathbf{S}_n^{\mathrm{Im}}\right]_{ij}/\partial r-V_N\sum\limits_n\left[\mathbf{S}_n^{\mathrm{Re}}\right]_{ij}/\partial r}\\
&=-\frac{U_N\sum\limits_n\left[\mathbf{S}_n^{\mathrm{Re}}\right]_{ij}\cdot\mathbf{d}_n\cdot\hat{\varphi}+V_N\sum\limits_n\left[\mathbf{S}_n^{\mathrm{Im}}\right]_{ij}\cdot\mathbf{d}_n\cdot\hat{\varphi}}{{U_N}^2+{V_N}^2}
\end{aligned}
\tag{12}
$$

where $[\mathbf{S}]_{ij}$ stands for the element of the matrix $\mathbf{S}$ in the ith row and jth column, and U_N, V_N, $\left[\mathbf{S}_n^{\mathrm{Re}}\right]_{ij}$ and $\left[\mathbf{S}_n^{\mathrm{Im}}\right]_{ij}$ degenerate into the far-field form,

$$\mathbf{S}'(r,\varphi,\theta,V,k) = \exp(-2jkr)\sum_n \mathbf{S}_{n,\varphi_n,\theta_n} \cdot \exp\left(2jk\mathbf{d}_n \cdot \hat{\mathbf{r}}\right) \tag{13}$$

(12) is consistent with the expression in [1], other than the definition of θ. Thus, the expression in [1] is a special case of (6) in the far field. (6) is obtained by the exact solution of the derivative of the backscattering phase vs. the position vector of the observer, and we call it the exact expression. Without the far-field assumption, it is applicable for any range, if the assumption in Section 2 is satisfied.

4. SIMPLIFIED EXPRESSION FOR TERMINAL GUIDANCE

As a calculating expression, (6) is fairly complicated. Combined with the terminal guidance radar, we simplify (6) in this section. As the presence of the radar blind range, we consider the distance ranging in

$$d_{\max}/\beta < r < 2 \cdot d_{\max}^2/\lambda \tag{14}$$

where β is the half-power beam width in radian, and $d_{\max}/\beta < r$ denotes that target angle is less than the mainlobe beam width.

With the constraint in (14), the far-field condition is not satisfied, but with the absence of incomplete irradiation. Thus we concentrate on the mainlobe beam in analysis. The pattern is usually approximated by

$$F(\psi) = \cos^q \psi \tag{15}$$

where $q = \log(1/\sqrt{2})/\log(\cos(\beta/2))$.

Substituting (15) into (9), we obtain

$$\begin{bmatrix} \partial \ln A_n/\partial r \\ \partial \ln A_n/\partial \varphi \\ \partial \ln A_n/\partial \theta \end{bmatrix} = 2\left(\frac{{r_n}^2 + r \cdot \mathbf{d}_n \cdot \hat{\mathbf{r}}}{r \cdot {r_n}^2}\begin{bmatrix}1\\0\\0\end{bmatrix} + \frac{1}{r_n}\left(\frac{r}{r_n} - \frac{q}{\cos\psi_n}\right) \cdot \begin{bmatrix} -1 \\ \cos\theta \cdot \mathbf{d}_n \cdot \hat{\varphi} \\ \mathbf{d}_n \cdot \hat{\theta} \end{bmatrix}\right) \tag{16}$$

For the terminal guidance radar sensor, generally β is set to a small angle ranging 2 6 degree to obtain good azimuth resolution, consequently, $q \gg 1$ and $r > d_{\max}/\beta \gg d_{\max}$. For example, if $\beta = 0.0873$ (5 degree), then $q \approx 370$ and $r > 11.5 d_{\max}$. For the nth scattering point, $1 - d_n/r \le r_n/r \le 1 + d_n/r$ can be obtained by

the triangular relationship. Therefore, $r/r_n \approx 1 \ll q$, and (16) can be simplified as

$$\begin{bmatrix} \partial \ln A_n/\partial r \\ \partial \ln A_n/\partial \varphi \\ \partial \ln A_n/\partial \theta \end{bmatrix} \approx -\frac{2q}{r_n \cos\psi_n} \begin{bmatrix} -1 \\ \cos\theta \cdot \mathbf{d}_n \cdot \hat{\varphi} \\ \mathbf{d}_n \cdot \hat{\theta} \end{bmatrix} \tag{17}$$

$\partial\alpha_n/\partial\mathbf{r}$ can be still approximated by (10) with $r/r_n \approx 1$ and $\mathbf{d}_n \cdot \hat{\mathbf{r}} \ll r$. Comparing $\partial\alpha_n/\partial\mathbf{r}$ in (17) with that in (10), $q/(r_n \cos\psi_n) \ll k$ is established in the considered distance range. It can be seen that the phase gradient aroused by the amplitude A_n is far less than that aroused by the phase α_n. Accordingly, the phase gradient because of A_n can be ignored in the calculation. Substituting (10) into (6), we can obtain the approximation as

$$\begin{aligned} e_\theta &= -\frac{(\mathbf{Rh}^r)^{\mathrm{T}} \left(U_N \sum_n \mathbf{S}_n^{\mathrm{Re}} \cdot \mathbf{d}_n \cdot \hat{\theta} + V_N \sum_n \mathbf{S}_n^{\mathrm{Im}} \cdot \mathbf{d}_n \cdot \hat{\theta} \right) \mathbf{Rh}^i}{{U_N}^2 + {V_N}^2} \\ &= -\frac{(\mathbf{Rh}^r)^{\mathrm{T}} \left(U_N \sum_n \mathbf{S}_n^{\mathrm{Re}} \cdot \mathbf{d}_n \cdot \hat{\theta} + V_N \sum_n \mathbf{S}_n^{\mathrm{Im}} \cdot \mathbf{d}_n \cdot \hat{\theta} \right) \mathbf{Rh}^i}{\left| (\mathbf{Rh}^r)^{\mathrm{T}} \mathbf{S} \cdot \mathbf{Rh}^i \right|^2} \\ e_\varphi &= -\frac{(\mathbf{Rh}^r)^{\mathrm{T}} \left(U_N \sum_n \mathbf{S}_n^{\mathrm{Re}} \cdot \mathbf{d}_n \cdot \hat{\varphi} + V_N \sum_n \mathbf{S}_n^{\mathrm{Im}} \cdot \mathbf{d}_n \cdot \hat{\varphi} \right) \mathbf{Rh}^i}{{U_N}^2 + {V_N}^2} \\ &= -\frac{(\mathbf{Rh}^r)^{\mathrm{T}} \left(U_N \sum_n \mathbf{S}_n^{\mathrm{Re}} \cdot \mathbf{d}_n \cdot \hat{\varphi} + V_N \sum_n \mathbf{S}_n^{\mathrm{Im}} \cdot \mathbf{d}_n \cdot \hat{\varphi} \right) \mathbf{Rh}^i}{\left| (\mathbf{Rh}^r)^{\mathrm{T}} \mathbf{S} \cdot \mathbf{Rh}^i \right|^2} \end{aligned} \tag{18}$$

Note that

1) Although both (18) and (12) are obtained based on the approximation of the derivative in (10), but they have different meanings; under the far-field condition, the approximation in (10) is very exact, but (18) has approximate error in the considered distance range.

2) Scattering matrix $\mathbf{S}$, $\mathbf{S}_n^{\mathrm{Re}}$, $\mathbf{S}_n^{\mathrm{Im}}$ and U_N, V_N in (18) are all defined at near field, but defined at far field in (12), which can be considered as the far-field approximation of (18). In this way, the expression in [1] can be extended in the near-field range, as long as the related parameters are replaced with their far-field forms.

3) In (18), $\left|(\mathbf{Rh}^r)^{\mathrm{T}} \mathbf{S} \cdot \mathbf{Rh}^i\right|^2$ is just the target near-field RCS [9].

5. SIMULATION

This section takes the angle glint calculation of F18 as an example to analyze the influencing factors and compare the exact expression in (6) and approximate expression in (18). The distance ranging in $100\,\mathrm{m} < r < 16000\,\mathrm{m}$, the half-power beam width is $\beta = 5^\circ$, $\lambda = 5\,\mathrm{cm}$, and polarization rotation angle is $\varepsilon_x = 0^\circ$. The scattering center mode of F18 shown in Figure 2 is obtained by the method in [10].

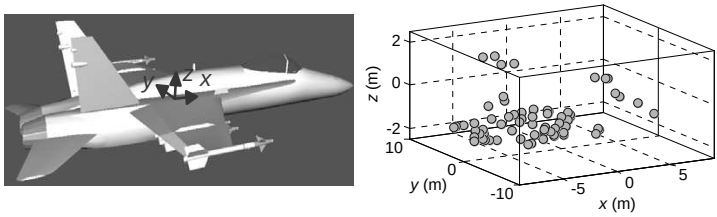

Figure 2. The scattering center mode of F18.

5.1. Analysis of Different Influencing Factors

From (6) (9), we can obtain that angle glint is related to distance r, incident direction (φ, θ), antenna pattern $F(\cdot)$, wavenumber k, transmitting and receiving polarization $(\mathbf{h}^r, \mathbf{h}^i)$, polarization rotation angle ε_x and so on. For a given radar system, $(\mathbf{h}^r, \mathbf{h}^i)$, $F(\cdot)$ and k are specified, and the main influencing factors become $(r, \varphi, \theta, \varepsilon_x)$. The effect of the factors on angle glint is described in Figure 3∼Figure 6, where $\mathbf{h}^i = \mathbf{h}^r = [1, 0]^{\mathrm{T}}$, and $F(\cdot)$ is calculated based on (15).

Figure 3 shows the four dimensional slices of angle glint vs. distance and incident angle, with $\varepsilon_x = 0$. We can observe that both in the azimuth slice and elevation slice, the angle glint makes the transition from strips of far range to spots of near range along the r direction, which shows the distance effect on angle glint. The relationship between them can be better observed in Figure 4(a), Figure 4(c), Figure 5(a) and Figure 5(c). The distance slice in Figure 3 describes the relationship between angle glint and incident angle. Comparing Figure 4(b), Figure 4(d), Figure 5(b), Figure 5(d) with Figure 4(a), Figure 4(c), Figure 5(a), Figure 5(c) respectively, it is not difficult to see that the sensitivity of angle glint to orientation is higher than that to distance. Moreover, as F-18 is with respect to the plane XOZ of symmetry, when $\varphi = 0$, we obtain $e_\varphi = 0$, which is clearly visible in Figure 4(c).

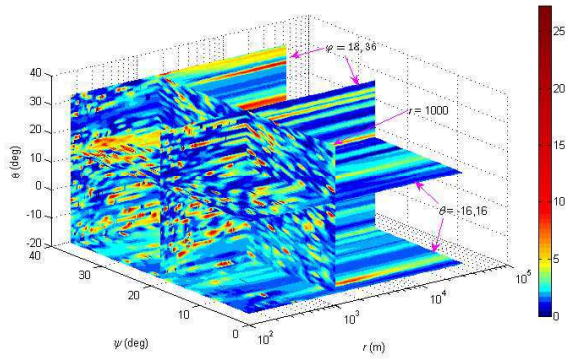

Figure 3. Slices of angle glint vs. distance and incident angle.

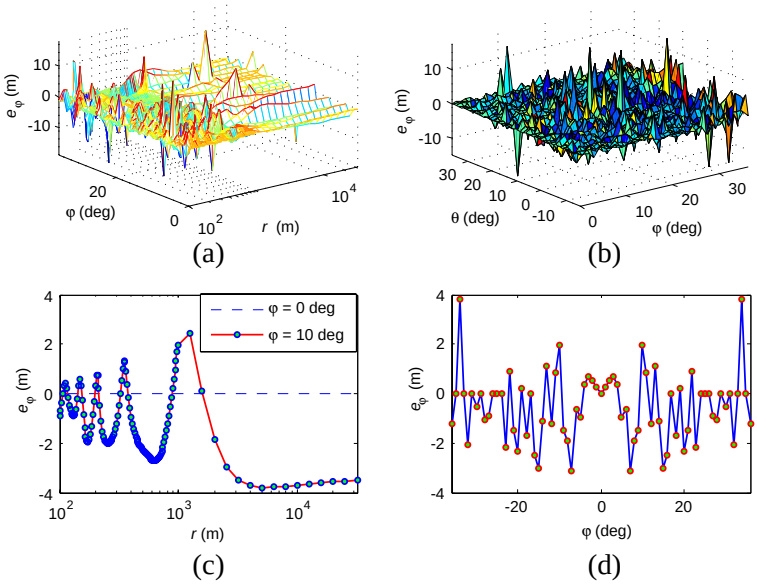

Figure 4. The relationship between e_φ and distance and orientation. (a) $\theta = 0$ deg. (b) $r = 1000$ m. (c) $\theta = 0$ deg. (d) $[r, \theta] = [1000, 0]$.

Figure 6 displays the effect of polarization rotation angle ε_x on line glint error e_φ, e_θ with $\varphi = 15°$ and $\theta = 0°$. It can be known from (6), for a specified polarization, ε_x affects e_φ and e_θ via the weighting factors of the scattering matrix, which leads to the periodicity shown in Figure 6.

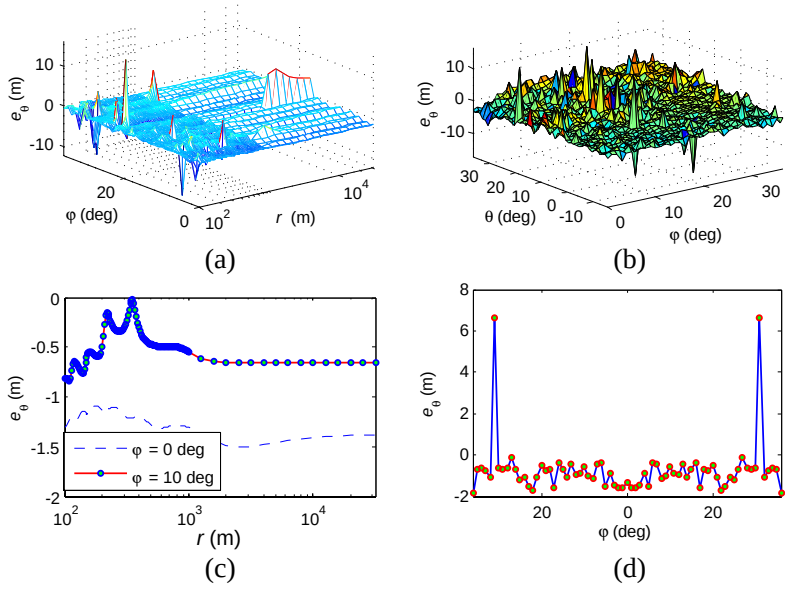

Figure 5. The relationship between e_θ and distance and orientation. (a) $\theta = 0$ deg. (b) $r = 1000$ m. (c) $\theta = 0$ deg. (d) $[r, \theta] = [1000, 0]$.

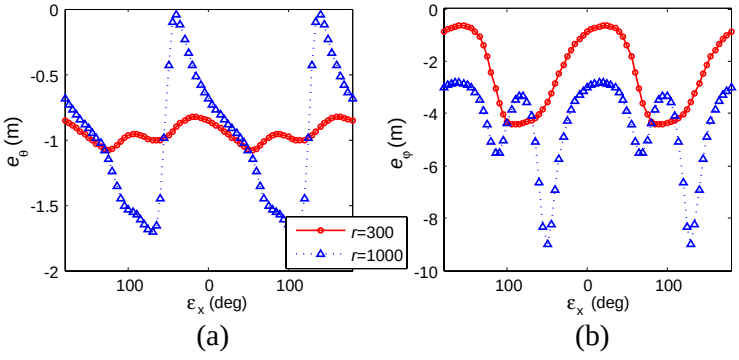

Figure 6. The effect of polarization rotation angle on angle glint.

Notice there are 315 junctions satisfying $|e_\theta| > 20$ and 714 junctions with $|e_\varphi| > 20$ in the space grids of Figure 3 ($116 \times 37 \times 53$). In consideration of clarity, the significant points with line glint error greater than 20 m are removed.

5.2. Error Analysis of the Approximate Expression

Define the approximate error in percent as

$$\Delta E = 100 \times \left| \frac{\sqrt{{e_{\theta 2}}^2 + {e_{\varphi 2}}^2} - \sqrt{{e_{\theta 1}}^2 + {e_{\varphi 1}}^2}}{\sqrt{{e_{\theta 1}}^2 + {e_{\varphi 1}}^2}} \right| \tag{19}$$

where the angle glints $e_{\theta 1}$, $e_{\varphi 1}$ are calculated by (6), while $e_{\theta 2}$, $e_{\varphi 2}$ are by (18).

Figure 7 plots the variation curves of the near-field angle glint obtained by (6) and (18) vs. distance, while Figure 8 represents the variation curves of the angle glint approximate error ΔE with each polarization transmitting and receiving pair vs. distance. It can be observed in Figure 8 that different from the far-field angle glint, the near-field angle glint depends on not only the incident angle but also the distance. In the near range of the distance, great fluctuation occurs in the angle glint with the change of distance. As the distance r increases, the angle glint gradually approaches to the far-field value and finally becomes independent of the distance. Besides, in the range of the considered distance, the two results obtained by the two expressions are almost consistent, which validate the approximate expression.

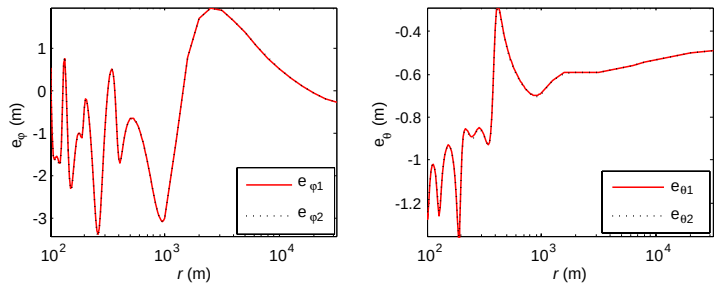

Figure 7. Near-field angle glint variation curves vs. distance. (a) HH polarization, $\epsilon_x = \theta = 0$, $\varphi = 15$ deg. (b) HH polarization, $\epsilon_x = \theta = 0$, $\varphi = 15$ deg.

Figure 8 shows the error distribution vs. distance. When $r > 300$ m, the approximate error is less than 1%. With the increase of distance r, the error approaches to 0. However, when $100\,\text{m} < r < 300\,\text{m}$, the error reaches 10% with the simulated orientation. As the distance r further decreases, the predictive approximate error will become much larger, but the distance has been in the blind range of radar sensor.

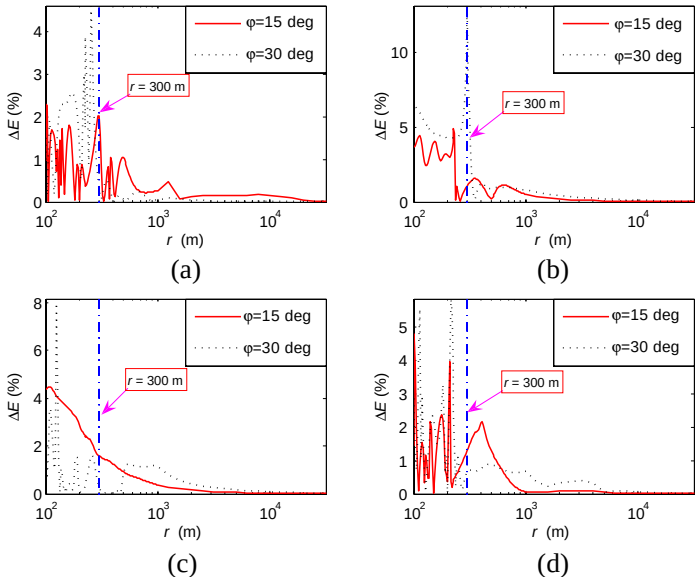

Figure 8. Approximate error ΔE variation curves vs. distance. (a) HH polarization, $\varepsilon_x = \theta = 0$. (b) HV polarization, $\varepsilon_x = \theta = 0$. (c) VH polarization, $\varepsilon_x = \theta = 0$. (d) VV polarization, $\varepsilon_x = \theta = 0$.

6. CONCLUSIONS

In this paper, we focus on the calculation of angle glint at near field. Based on the phase gradient method, we derive the exact expression of angle glint, which is applicable for the far-field angle glint. Theoretical analysis shows that the angle glint expression in [1] is just the far-field approximation of the derived expression under specified polarization. Combined with the terminal guidance, we demonstrate that in the range of considered distance, the amplitude impact on the phase gradient can be ignored, and gives the responding approximate expression. Eventually, we analyze the effect of each factor on angle glint by simulation, and the approximate error between the simplified and exact expressions. The relative results obtained in this study could be adopted as some theoretical basis for the estimation and investigation of the near-field angle glint.

ACKNOWLEDGMENT

We appreciate the support from the National Natural Science Foundation of China (Grant Number: 61101186) and Dr. Jianxiong Zhou for providing multiple-scatter model data of F18.

REFERENCES

1. Huang, P. K., G. S. Lin, et al., *Radar Target Signature*, Astronautics Publishing House, Beijing, China, 1993.
2. Yin, H. C., S. H. Deng, Y. Z. Ruan, et al., "On the conditions for obtaining angular glint by backscattering echo relative phase," *Acta Electronica Sinica*, Vol. 24, No. 9, 36–40, 1996.
3. Bilik, I. and J. Tabrikian, "Target tracking in glint noise environment using nonlinear non-Gaussian Kalman filter," *IEEE Conference on Radar*, 282–287, 2006.
4. Chang, D. C. and W. R. Wu, "Feedback median filter for robust preprocessing of glint noise," *IEEE Transactions on Aerospace and Electronic Systems*, Vol. 36, No. 4, 1026–1035, 2000.
5. Hughes, E. J. and M. Leyland, "Target manoeuvre detection using radar glint," *Electronics Letters*, Vol. 34, No. 17, 1695–1696, 1998.
6. Jeng, S. K., "Near-field scattering by physical theory of diffraction and shooting and bouncing rays," *IEEE Transactions on Antennas and Propagation*, Vol. 46, No. 4, 551–558, 1998.
7. Li, X. J. and J. Li, "An algorithm of near field RCS of complex objects," *Guidance and Fuze*, Vol. 26, No. 3, 47–51, 2005.
8. Bhalla, R. and H. Ling, "Near-field signature prediction using far-field scattering centers extracted from the shooting and bouncing ray technique," *IEEE Transactions on Antennas and Propagation*, Vol. 48, No. 2, 337–338, 2000.
9. Taylor, J. M. and A. J. Terzuoli, "On the concept of near field radar cross section," *IEEE Antennas and Propagation Society International Symposium*, Vol. 2, 1172–1175, Montreal, Que., Canada, 1997.
10. Zhou, J., H. Zhao, Z. Shi, and Q. Fu, "Global scattering center model extraction of radar targets based on wideband measurements," *IEEE Transactions on Antennas and Propagation*, Vol. 56, No. 7, 2051–2060, 2008.